*Korean J. Chem. Eng.*, **31**(11), 2051-2056 (2014)
DOI: 10.1007/s11814-014-0162-8

pISSN: 0256-1115
eISSN: 1975-7220

# Adsorption and photodegradation of methylene blue on $TiO_2$-halloysite adsorbents

**Yuanyuan Du and Pengwu Zheng†**

School of Pharmacy, Jiangxi Science and Technology Normal University, Nanchang, Jiangxi 330013, China
(*Received 31 March 2014 • accepted 12 June 2014*)

**Abstract**−$TiO_2$-halloysite ($TiO_2$-HNT) composites were fabricated by depositing anatase $TiO_2$ on the halloysite (HNT) surfaces with calcination treatment at 100, 200, 300 and 500 °C. The obtained composites were characterized by transmission electron microscopy (TEM), Fourier transform infrared spectroscopy (FTIR) and X-Ray diffraction (XRD). HNT was attached with $TiO_2$ particles or clusters in sizes of 10-30 nm. With the increasing of calcination temperature, the crystalline of anatase became more perfect, but the structure of HNT could be destroyed at 500 °C. The adsorption and photodegradation of methylene blue (MB) by $TiO_2$-HNTs were investigated. The kinetic adsorption fit the pseudo second-order, and the isotherm data followed the Langmuir model. The maximum adsorption capacities of MB were in the range of 38.57 to 54.29 mg/g. $TiO_2$-HNTs exhibited an efficient photocatalytic activity in the decomposition of MB. For $TiO_2$-HNT calcined at 300 °C, 81.6% MB were degraded after 4 h treatment of UV irradiation.

Keywords: Halloysite, $TiO_2$, Methylene Blue, Adsorption, Photodegradation

## INTRODUCTION

Dyes are extensively used in textiles, rubber, plastics, paper, leather, cosmetics, pharmaceuticals and food industries [1]. Since dyes are known pollutants, the effluents of textile and related industry have to be treated carefully before discharge. The treatment and disposal of dye-contaminated wastewater is one of the most serious environmental problems. This has resulted in a demand to remove the dyes from effluents [2]. Researchers have removed toxic dyes from wastewater using various adsorbents such as activated carbons, carbon nanotubes, graphene oxide, zeolites, clays, industrial by-products, agricultural waste, biomass and polymeric materials [3].

Halloysite nanotube (HNT) is a kind of aluminosilicate clay mined from natural deposits [4]. HNT possesses a two-layer structure formed by a corner sharing [$SiO_4$] tetrahedral layer and an edge sharing [$AlO_6$] octahedral layer. Each of these two layers is separated by a monolayer of interlayer water molecules [5]. Because HNTs possess some excellent characteristics, such as large surface area, large pore volume and adequate hydroxyl groups [6], HNTs have been used as catalytic support [7], for storing hydrogen, removal of environmental hazardous species and diuretic drug delivery [8]. As adsorbents, HNTs are also proven to be able to remove cationic dyes [4,9] and Cr (VI) [6] due to large surface area.

The development of photocatalysis has recently gained considerable attention in environmental-related fields. $TiO_2$ has been the most widely studied and used in the decomposition of organic pollutants because of strong oxidizing abilities, chemical stability, long durability, nontoxicity, low cost, and transparency to visible light [10]. In aqueous dispersions, clay minerals have been composited with $TiO_2$ to enhance the removal of organic pollutants by photocatalytic degradation. Rectorite layers were intercalated by colloidal titania particles to improve photocatalytic activity in the decomposition of the dye acid red G by UV light irradiation [11]. $TiO_2$/HNTs composites have been prepared to obtain the photocatalytic activities in decomposing $NO_x$ gas, toluene [12], methanol and acetic acid [13]. In this work, $TiO_2$ was incorporated to HNTs to prepare the $TiO_2$-HNT composites, which were treated with different calcinations temperatures. The effect of calcination temperature on the structures and the properties of $TiO_2$-HNTs would be evaluated. The cationic methylene blue (MB) dye was adsorbed on $TiO_2$-HNTs. The photogenerated charge carriers (hole and electron) on $TiO_2$ can make the adsorbed MB dye incur photodegradation. This is a self-cleaning process, and $TiO_2$-HNTs can continue to adsorb the dye and degrade the dye.

## MATERIALS AND METHODS

### 1. Materials

The HNTs were obtained from Hunan province, China. MB dye was provided by Tianjin Benchmark Chemical Reagent Co., Ltd. All other reagents were commercially available and of analytical grade.

### 2. Preparation of $TiO_2$-HNTs

Tetrabutyl titanate, $Ti(OC_4H_9)_4$ (7.2 g) was added in 20 mL absolute ethanol. The mixture was stirred for 15 min at the room temperature, followed by the addition of 3 g acetic acid and stirred for another 15 min. HNT (3 g) was slowly added to the mixture, and the suspension was stirred for 1 h at 30 °C. The solution, composed of 1.7 g $NH_4NH_3$, 6 mL distilled water and 5 mL absolute ethanol, was added dropwise and the pH was controlled in the range of 2-3. The mixture reacted for 2 h at 40 °C in a sealed container, and was stored at the room temperature for another 5 h. The products ($TiO_2$-HNTs) were centrifuged and oven-dried for 3 h at 100 °C. $TiO_2$-HNTs were calcined in Muffle furnace for 2 h at 200 °C, 300 °C and 500 °C in air. They were respectively marked as $TiO_2$-HNT-200, $TiO_2$-HNT-300 and $TiO_2$-HNT-500.

†To whom correspondence should be addressed.
E-mail: zhengpw@126.com

### 3. Characterization

The morphology was tested with transmission electron microscopy (TEM). Drops of $TiO_2$-HNT aqueous suspensions were delivered onto the copper grid and air dried. The samples were analyzed using a TEM JEM-1200EX. And the atomic weight of Zn for $TiO_2$-HNT-300 was recorded with energy dispersive X-ray spectroscopy (EDS).

Fourier transform infrared spectroscopy (FTIR) spectra of HNT and $TiO_2$-HNTs were obtained on a BIO-RAD FTS3000 IR Spectrum Scanner.

HNT and $TiO_2$-HNT powders were placed in a sample holder for X-ray diffraction (XRD). XRD patterns were recorded in reflection mode in the angular range of 10-70° ($2\theta$), at ambient temperature, by Bruker D8-S4 Pioneer operated at a CuK$\alpha$ wavelength of 1.542 Å.

### 4. MB Adsorption Experiments

Adsorption experiments were performed using glass bottles containing 1 g/L of adsorbents and dye (0.1 mmol/L MB). The glass bottles were placed on a slow-moving platform shaker at 25 °C, 35 °C and 45 °C, respectively. MB concentrations in the solution were analyzed by UV-Vis spectrometry at different time intervals during the reaction.

In adsorption isotherm testing, the concentration of the adsorbents was 1 g/L, and MB concentrations changed from 0.01 to 0.3 mmol/L. The experiment was conducted at 25 °C, and all suspensions were shaken at 100 rpm for 24 h to reach the adsorption equilibrium.

### 5. Photodegradation Experiments

The glass bottles containing 0.5 g/L of adsorbents and MB dye (0.1 mmol/L) were shaken at 100 rpm for 24 h to reach the adsorption equilibrium at 25 °C. The glass bottles were exposed to UV irradiation at 25 °C. The UV light source was a 12 W UV lamp ($\lambda$= 365 nm), and the irradiation intensity was approximately 350 μW/cm$^2$. At some time intervals (about 1 h), MB concentrations were evaluated using a UV-vis spectrometer. The degree of degradation is expressed by $(C_0-C_t)/C_0$ [14]. Here $C_0$ is the MB concentration before UV irradiation, and $C_t$ is MB concentrations after a period

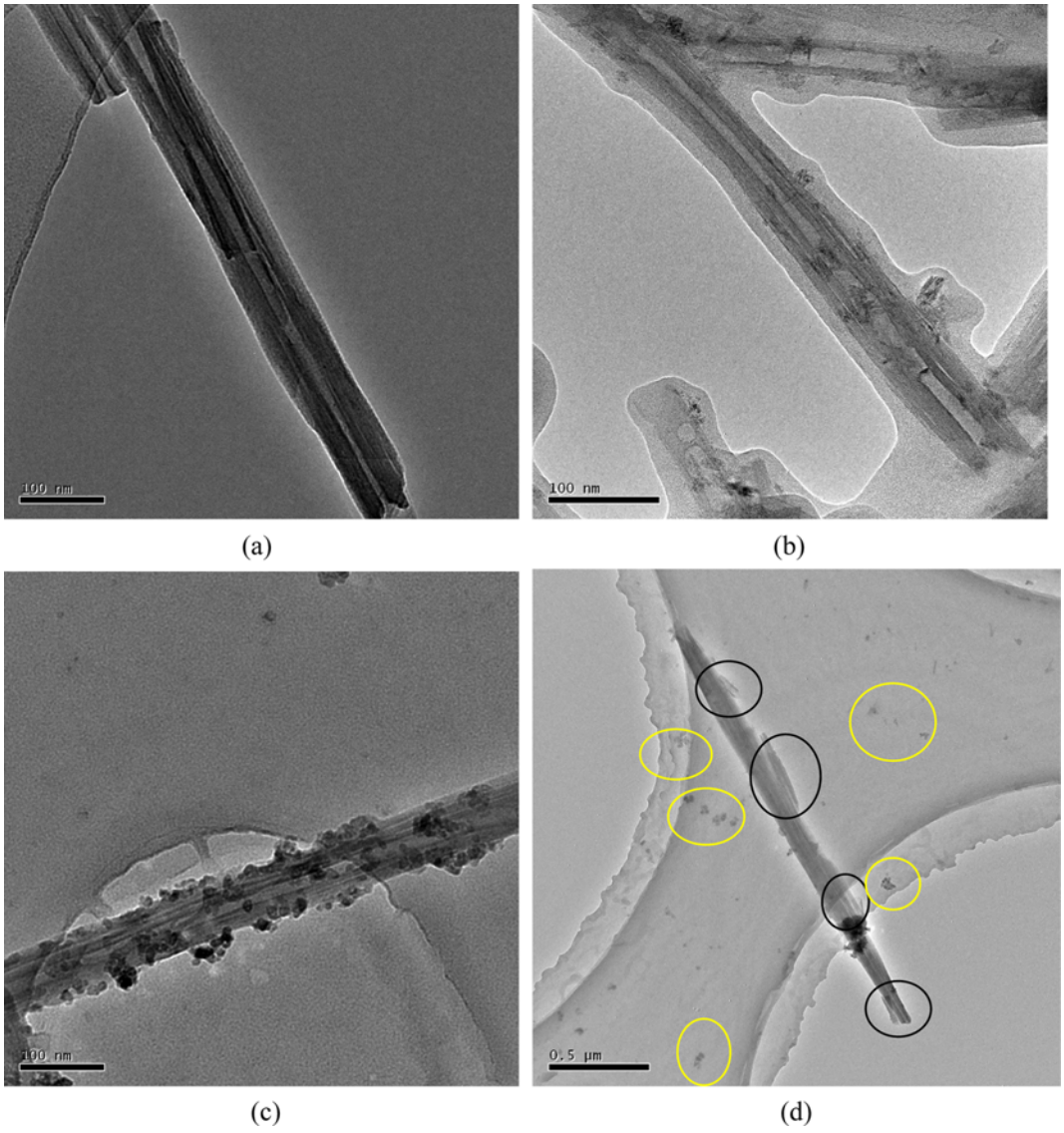


**Fig. 1. TEM micrographs for HNT (a), $TiO_2$-HNT-100 (b), $TiO_2$-HNT-300 (c) and $TiO_2$-HNT-500 (d).**

of exposed time (accumulation of time intervals).

## RESULTS AND DISCUSSION

### 1. Characterization of $TiO_2$-HNTs

As shown in Fig. 1, the morphologies of HNT and $TiO_2$-HNTs were obtained by TEM. HNTs (Fig. 1(a)) exhibited the nanotubes with the smooth surface, open ends and hollow cavity of about 10-20 nm in diameter. In Fig. 1(b), the surface of $TiO_2$-HNT-100 seemed be covered with organic material, butanol, sourcing from the hydrolysis of tetrabutyl titanate. In Fig. 1(c) for $TiO_2$-HNT-300, at the high calcination temperature (300 °C), organic materials were burnt away and $TiO_2$ particles were clearly observed. HNT was attached with $TiO_2$ particles or clusters in sizes of 10-30 nm. $TiO_2$ clusters were composed of even smaller subunits of about 10 nm, indicating that the large clusters may be formed from the precipitation followed by a step-like aggregation process. And some $TiO_2$ particles even entered the hollow cavity of HNT. At the higher calcination temperature (500 °C), HNT structures could be destroyed, and some fragments were found, as marked with black circles in Fig. 1(d). And many $TiO_2$ particles, marked as yellow circles, were also found to fall down from HNTs. The atomic weight of Ti (7.6 wt%) for $TiO_2$-HNT-300 was recorded by EDS in TEM testing. The content of $TiO_2$ in $TiO_2$-HNTs was calculated to be about 12.7 wt%.

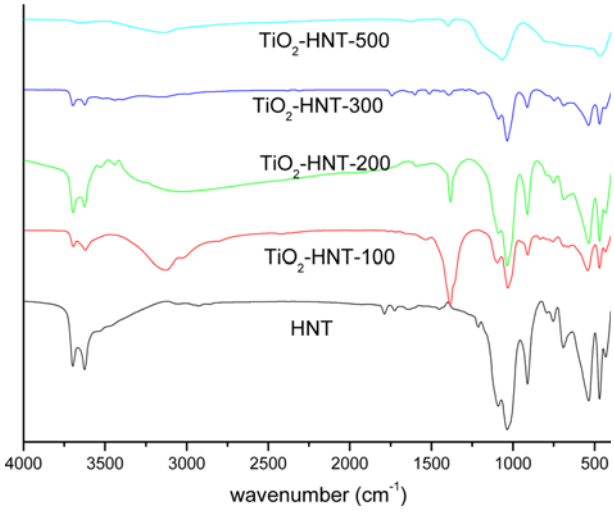


**Fig. 2. FTIR spectra of HNT and $TiO_2$-HNTs.**

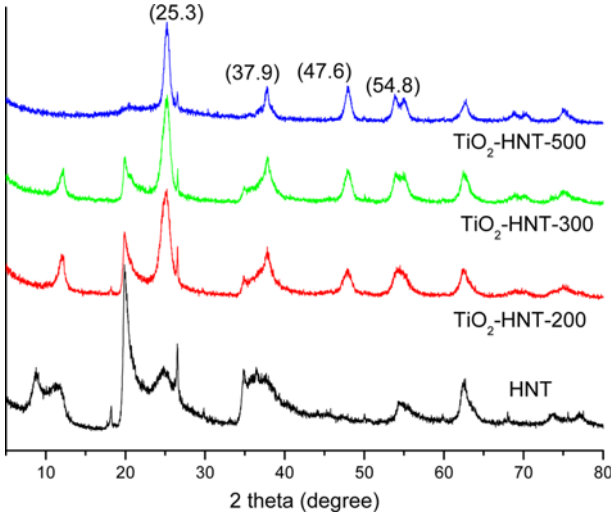


**Fig. 3. X-ray diffraction patterns of HNT and $TiO_2$-HNTs.**

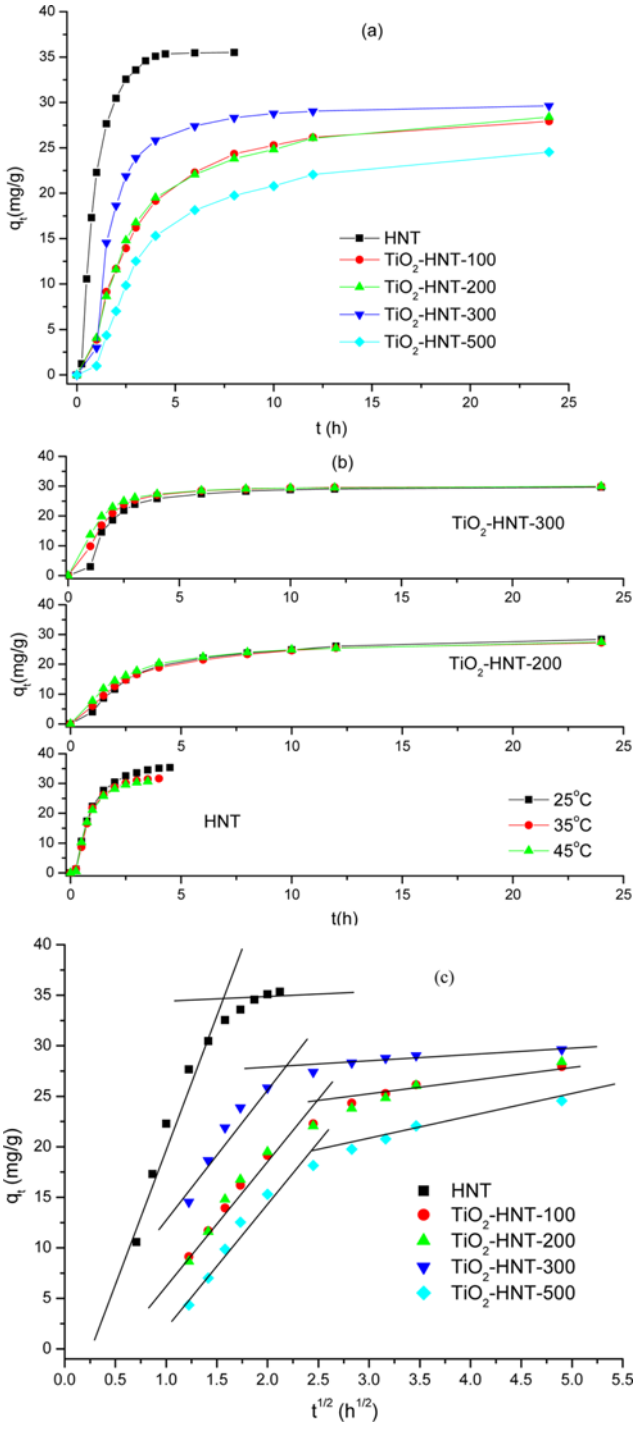


**Fig. 4. The adsorption of MB on HNT and $TiO_2$-HNTs. (a) Effect of contact time and calcination temperature on adsorption of MB at 25 °C. (b) Effect of adsorption temperatures on adsorption of MB. (c) The intra-particle model for adsorption of MB at 25 °C. Initial concentration: MB 37.39 mg/L; HNT or $TiO_2$-HNTs 1 g/L.**

Fig. 2 exhibits the FTIR spectra of HNT and $TiO_2$-HNTs. The double peaks at 3,696 and 3,623 $cm^{-1}$ were due to the stretching vibrations of Al-OH groups at the surface of HNTs [9,15]. The deformation of Al-O-Si and O-H deformation of inner hydroxyl groups exhibited the peaks at 536 and 910 $cm^{-1}$, respectively [16]. The above-mentioned peaks all appeared in FTIR of $TiO_2$-HNTs except for $TiO_2$-HNT-500, in which HNT structure could be destroyed. The peaks near 1,000 $cm^{-1}$ were assigned to Si-O groups in HNT. The peak at 1,390 $cm^{-1}$ was related to C-H groups of butanol in $TiO_2$-HNT-100 and $TiO_2$-HNT-200. And the $TiO_2$ characteristic peak at around 1,000-600 $cm^{-1}$ [17] could be overlapped with HNT in $TiO_2$-HNTs.

The XRD patterns of the HNT and $TiO_2$-HNTs are shown in Fig. 3. The powder XRD patterns of $TiO_2$-HNTs displayed distinct peaks at $2\theta$ values of about 25.3, 37.9, 47.6, 54.8 and 62.7 [12], as marked in Fig. 3. The XRD patterns of $TiO_2$-HNTs exhibited all the characteristic reflections of anatase ($TiO_2$). With the increasing of calcination temperature (from 100 to 500 °C), the above listed peaks were sharpened, and the crystalline of anatase became more perfect. In $TiO_2$-HNT-500, the disappearance of the peaks of HNT at $2\theta$ values of about 10 and 20 indicated that the high calcination temperature (500 °C) destroyed the structure of HNT. This is consistent with the FTIR and TEM results.

## 2. MB Adsorption

### 2-1. Effect of Contact Times and Adsorption Temperatures

Fig. 4(a) illustrates the effects of contact time and calcination temperature on adsorption of MB by HNT and $TiO_2$-HNTs. The amounts of MB dye adsorbed at equilibrium ($q_e$) are listed in Table 1. There are obvious differences in the experimental $q_e$ data and the adsorbed times at equilibrium ($T_{eq}$) among HNT (35.35 mg/g and 4 h) and $TiO_2$-HNT-100 (27.94 mg/g and 12 h), $TiO_2$-HNT-200 (28.39 mg/g and 12 h), $TiO_2$-HNT-300 (29.64 mg/g and 12 h) and $TiO_2$-HNT-500 (24.55 mg/g and 12 h). The incorporation of $TiO_2$ covered the surface of HNT, decreased the adsorption capacity for MB dye and delayed the $T_{eq}$. The high calcination temperature (500 °C) could destroy the structure of HNT and obviously decreased the adsorption capacity.

As shown in Fig. 4(b), the influence of adsorption temperature on MB adsorption was also investigated. HNT exhibited better MB adsorption at the lower adsorption temperature, so the process was exothermic. But the adsorption capacity at equilibrium of HNT only varied a little from to 35.35 to 30.68 mg/g, when the adsorption temperature increased from 25 °C to 45 °C. The introduction of $TiO_2$ particles further weakened the dependence of MB adsorption on the adsorption temperatures. It could be related to the coverage of $TiO_2$ on the adsorption sites of HNT.

### 2-2. Batch Adsorption Kinetic Modeling

The pseudo-first-order kinetic model is not suitable to describe the adsorption process (not shown here), so the adsorption process was studied in the pseudo-second-order kinetic model and the intra-particle diffusion model. According to these models, the equations are expressed as:

$$\frac{t}{q_t} = \frac{1}{kq_e^2} + \frac{t}{q_e} \quad (2)$$

$$q_t = K_{id}t^{1/2} + C \quad (3)$$

where k (mg/g h) is the second-order rate constant, $q_t$ (mg/g) is the amounts of dye adsorbed at time t (h) and $q_e$ (mg/g) represents the amounts of dye adsorbed at equilibrium; $K_{id}$ (mg/g $h^{1/2}$) is the intra-particle diffusion rate constant and C is the intercept.

Some kinetic constants from pseudo-second-order kinetic model were estimated from the experimental data in Fig. 4(b), and listed in Table 1. The adsorption process for HNT and $TiO_2$-HNTs could fit well the pseudo second-order model with high correlation coefficients (R>0.997), but the linear relationship between $t/q_t$ and t (R= 0.974) was worse in the whole adsorption process for $TiO_2$-HNT-500.

According to the intra-particle diffusion model, there was two-linearity (i.e., two step adsorption process) in Fig. 4(c). The sharper first stage was related to the diffusion of MB molecules from the aqueous solution to the external surface of adsorbent or the boundary layer diffusion of MB molecules. The second stage exhibited gradual adsorption until equilibrium was reached. The linear portion of the first stage did not pass though the origin, indicating a boundary layer resistance existed between adsorbent and adsorbate [18]. As shown in Table 1, the slopes of the line of the first stage (i.e., the intra-particle diffusion rate constant) for all $TiO_2$-HNTs were very close between 10.10-11.46 mg/g $h^{1/2}$, which was much lower than that (24.56 mg/g $h^{1/2}$) of HNT. The introduction of $TiO_2$ decreased the diffusion rate constants, but calcination temperatures had little effect on the diffusion rate constants.

### 2-3. Batch Adsorption Isotherm Modeling

The adsorption isotherm for MB by HNT and $TiO_2$-HNTs is displayed in Fig. 5(a). At low values of the equilibrium concentration ($C_e$ (mg/L)), $q_e$ increased quickly with the increasing of $C_e$, while $q_e$ had the little dependence of MB adsorption on $C_e$ at the high $C_e$. The Langmuir model is widely used to describe the adsorption isotherms and investigate mechanisms of adsorption. The equation is as follows:

$$\frac{C_e}{q_e} = \frac{1}{bq_{max}} + \frac{C_e}{q_{max}} \quad (4)$$

**Table 1. Kinetic and isothermal constants for MB adsorption by HNT and $TiO_2$-HNTs at 25 °C**

| | Experiment | Pseudo-second-order model | | | Intra-particle diffusion model | | Langmuir constants | | |
|---|---|---|---|---|---|---|---|---|---|
| | $q_e$ (mg/g) | k (g/mg h) | $q_e$ (mg/g) | R | $K_{id}$ (mg/g $h^{1/2}$) | R | b (L/mg) | $q_{max}$ (mg/g) | R |
| HNT | 35.50 | 0.024 | 43.73 | 0.997 | 24.56 | 0.974 | 0.49 | 97.56 | 0.999 |
| $TiO_2$-HNT-100 | 27.94 | 0.010 | 32.06 | 0.998 | 10.88 | 0.984 | 1.57 | 44.31 | 0998 |
| $TiO_2$-HNT-200 | 28.39 | 0.010 | 32.48 | 0.998 | 10.94 | 0.970 | 0.42 | 54.29 | 0.999 |
| $TiO_2$-HNT-300 | 29.65 | 0.029 | 31.33 | 0.999 | 10.10 | 0.929 | 0.64 | 49.73 | 0.999 |
| $TiO_2$-HNT-500 | 24.55 | 0.010 | 28.16 | 0.974 | 11.46 | 0.977 | 0.15 | 38.57 | 0.978 |

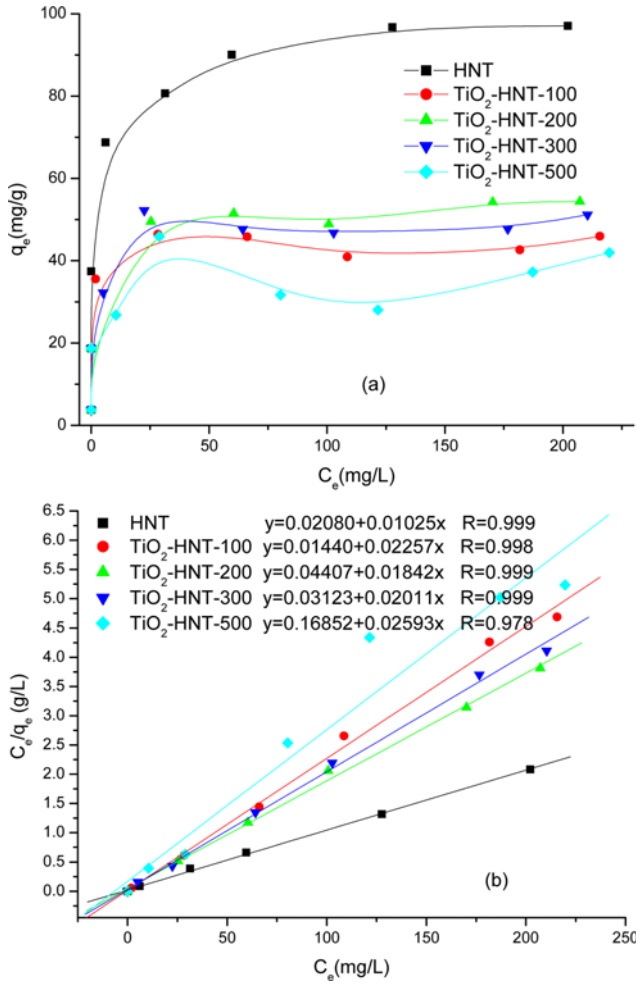


**Fig. 5. Adsorption isotherms (a) and the Langmuir model (b) for batch adsorption of MB on HNT and $TiO_2$-HNTs at 25 °C.**

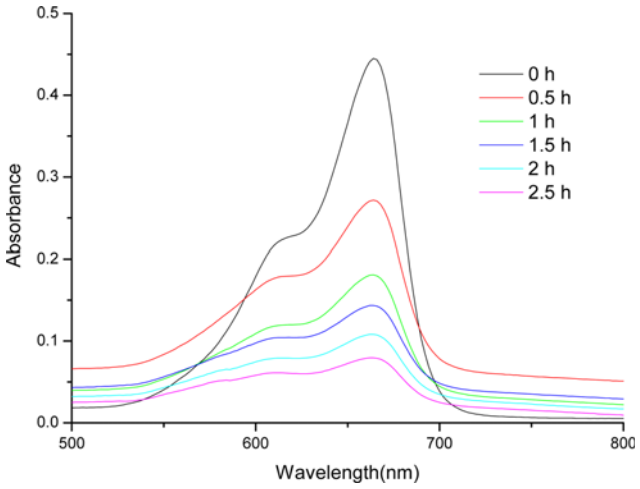


**Fig. 6. Spectra of MB aqueous solution exposed under UV irradiation for different irradiation times in the present of $TiO_2$-HNT-300.**

where $q_{max}$ (mg/g) is the maximum monolayer adsorption capacities, b (L/mg) is the Langmuir adsorption equilibrium constant.

The parameters from the Langmuir isotherm were obtained from Fig. 5(b) and listed in Table 1. The adsorption of $TiO_2$-HNTs fitted the Langmuir model well because of R≈1. This result demonstrated that a monolayer of MB covered the surface after adsorption. The maximum monolayer adsorption capacities ($q_{max}$) were 44.31, 54.29, 49.73 and 38.57 mg/g for $TiO_2$-HNT-100, $TiO_2$-HNT-200, $TiO_2$-HNT-300 and $TiO_2$-HNT-500, respectively. The $q_{max}$ values of $TiO_2$-HNTs were much lower than HNT. It indicated that introduction of $TiO_2$ could occupy the adsorption sites on the surface of HNT, and the calcinations could decrease the adsorption capacity of HNT. The $q_{max}$ values of $TiO_2$-HNTs are still competitive with other adsorbents including rectorite-$Fe_3O_4$ (31.18 mg/g) [19], HNT-$Fe_3O_4$ (18.64 mg/g) [20] and wheat shells (16.56 mg/g) [21].

Table 2 lists the errors on slope and intercept for pseudo-second-order, intra-particle diffusion and Langmuir models.

## 3. Photodegradation

Fig. 6 shows the effect of exposure times on spectra of MB solution in the presence of $TiO_2$-HNT-300 and UV irradiation. The maximal absorbance at 662 nm decreased from 0.45 to 0.07 as the exposure time increased from 0 to 2.5 h. It indicated that $TiO_2$-HNT-300 had photocatalytic activity or could degrade MB dye with the N-demethylation by $TiO_2$ of $TiO_2$-HNT-300 in a stepwise process in UV irradiation [22].

The photocatalytic activity of $TiO_2$-HNTs was evaluated by the degradation of MB dye. Fig. 7 shows the degradation of MB by $TiO_2$-HNTs, which were calcined under different temperatures. $TiO_2$-HNT-300 exhibited a high photocatalytic activity for the decomposition of MB dye (81.6% after 4 h) in aqueous solution under UV-light irradiation. The calcination temperature had a great effect on the photocatalytic activity of $TiO_2$-HNTs. With the increasing of calcination temperatures from 100 to 300 °C, the photodegradation of MB (i.e., photocatalytic activity of $TiO_2$-HNTs) increased considerably. As shown in XRD, at higher calcination temperature the crystalline of anatase became more perfect, which supported the photocatalytic activity. However, $TiO_2$-HNT-500 exhibited lower

**Table 2. The errors on slope and intercept for Pseudo-second-order, intra-particle diffusion and Langmuir models**

| | Pseudo-second-order model | | | Intra-particle diffusion model | | | Langmuir constants | | |
|---|---|---|---|---|---|---|---|---|---|
| | Slope | Intercept | $R^2$ | Slope | Intercept | $R^2$ | Slope | Intercept | $R^2$ |
| HNT | 0.023±6.35×10$^{-4}$ | 0.022±1.79×10$^{-3}$ | 0.994 | 24.56±2.83 | −4.32±3.32 | 0.937 | 0.010±1.41×10$^{-4}$ | 0.021±1.23×10$^{-2}$ | 0.999 |
| $TiO_2$-HNT-100 | 0.031±7.18×10$^{-4}$ | 0.094±7.03×10$^{-3}$ | 0.995 | 10.88±0.86 | −3.46±1.53 | 0.969 | 0.023±5.68×10$^{-4}$ | 0.014±6.24×10$^{-2}$ | 0.996 |
| $TiO_2$-HNT-200 | 0.031±7.16×10$^{-4}$ | 0.097±7.01×10$^{-3}$ | 0.995 | 10.94±1.36 | −3.42±2.42 | 0.927 | 0.018±4.08×10$^{-4}$ | 0.044±4.53×10$^{-2}$ | 0.997 |
| $TiO_2$-HNT-300 | 0.032±4.95×10$^{-4}$ | 0.035±4.84×10$^{-3}$ | 0.998 | 10.10±2.02 | 4.53±3.59 | 0.828 | 0.020±4.22×10$^{-4}$ | 0.031±4.49×10$^{-2}$ | 0.997 |
| $TiO_2$-HNT-500 | 0.036±0.003 | 0.122±0.032 | 0.942 | 11.46±1.25 | −8.68±2.22 | 0.944 | 0.026±2.28×10$^{-3}$ | 0.169±0.26 | 0.948 |

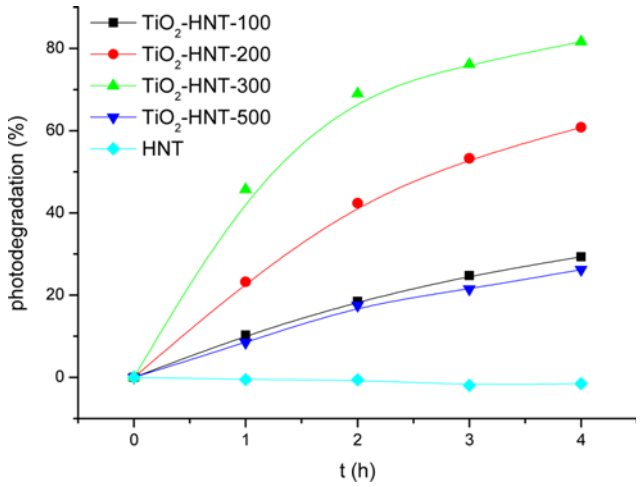


**Fig. 7. Photocatalytic degradation of MB on HNT and $TiO_2$-HNTs.**

photocatalytic activity than $TiO_2$-HNT-300. It could be related to the destroyed HNT structure with lower adsorption. Therefore, the high photocatalytic efficiency could be attributed to both the adsorption of the dye on HNT surface and the catalytic activity of $TiO_2$ particles [11]. When MB was accumulated on HNT due to the adsorption, MB with high concentration was easily degraded by $TiO_2$ particles.

## CONCLUSIONS

$TiO_2$ nanoparticles were synthesized on HNT to prepare self-cleaning adsorbents by hydrolyzing tetrabutyl titanate, and then calcined at the different temperatures. The introduction of $TiO_2$ particles further weakened the dependence of MB adsorption on the adsorption temperatures. With the increasing of temperature, the calcination treatments could produce complete anatase crystalline but destroy the structure of HNT. The incorporation of $TiO_2$ decreased adsorption capacity but endowed $TiO_2$-HNTs with photodegradation capacity. $TiO_2$-HNT-300 exhibited the high photocatalytic efficiency, which could be ascribed to both the adsorption of the dye on HNT surface and the catalytic activity of $TiO_2$ particles. $TiO_2$-HNT by calcination treatments could have a bright perspective on the photodegradation of the contaminants in water.

## ACKNOWLEDGEMENTS

This research was supported by the Science and Technology Project of Jiangxi Provincial Office of Education (KJLD12082, GJJ12590, and Innovation Platform "project 311") and Nature Science Foundation of Jiangxi Province (20132BAB 206006) and the National Nature Science Foundation of China (51162011).

## REFERENCES

1. K. Belkassa, F. Bessaha, K. Marouf-Khelifa, I. Batonneau-Gener, J. Comparot and A. Khelifa, *Colloids Surf., A*, **421**, 26 (2013).
2. J. L. Gong, B. Wang, G. M. Zeng, C. P. Yang, C. G. Niu, Q. Y. Niu, W. J. Zhou and Y. Liang, *J. Hazard. Mater.*, **164**, 1517 (2009).
3. G. Crini, *Bioresour. Technol.*, **97**, 1061 (2006).
4. M. F. Zhao and P. Liu, *Micropor. Mesopor. Mater.*, **112**, 419 (2008).
5. A. B. Zhang, L. Pan, H. Y. Zhang, S. T. Liu, Y. Ye, M. S. Xia and X. G. Chen, *Colloids Surf., A*, **396**, 182 (2012).
6. J. H. Wang, X. Zhang, B. Zhang, Y. F. Zhao, R. Zhai, J. D. Liu and R. F. Chen, *Desalination*, **259**, 22 (2010).
7. M. Massaro, S. Riela, G. Cavallaro, M. Gruttadauria, S. Milioto, R. Noto and G. Lazzara, *J. Organomet. Chem.*, **749**, 410 (2014).
8. M. H. Shamsi and K. E. Geckeler, *Nanotechnology*, **19**, 075604 (2008).
9. P. Luo, Y. F. Zhao, B. Zhang, J. D. Liu, Y. Yang and J. F. Liu, *Water Res.*, **44**, 1489 (2010).
10. K. Nakata and A. Fujishima, *J. Photochem. Photobiol. C*, **13**, 169 (2012).
11. Y. L. Zhang, Y. D. Guo, G. K. Zhang and Y. Y. Gao, *Appl. Clay Sci.*, **51**, 335 (2011).
12. D. Papoulis, S. Komarneni, D. Panagiotaras, E. Stathatos, D. Toli, K. C. Christoforidis, M. Fernández-García, H. Li, S. Yin, T. Sato and H. Katsuki, *Appl. Catal. B*, **132-133**, 416 (2013).
13. R. J. Wang, G. H. Jiang, Y. W. Ding, Y. Wang, X. K. Sun, X. H. Wang and W. X. Chen, *ACS Appl. Mater. Inter.*, **3**, 4154 (2011).
14. M. Sookhakian, Y. M. Amin and W. J. Basirun, *Appl. Clay Sci.*, **283**, 668 (2013).
15. Y. Zhang, L. J. Fu and H. M. Yang, *Colloids Surf., A*, **414**, 115 (2012).
16. E. Tierrablanca, J. Romero-García, P. Roman and R. Cruz-Silva, *Appl. Catal. A*, **381**, 267 (2010).
17. Y. Zhang, A. Barber, J. Maxted, C. Lowe, R. Smith and T. Z. Li, *Prog. Org. Coat.*, **76**, 131 (2013).
18. L. Liu, Y. Z. Wan, Y. D. Xie, R. Zhai, B. Zhang and J. D. Liu, *Chem. Eng. J.*, **187**, 210 (2012).
19. D. L. Wu, P. W. Zheng, P. R. Chang and X. F. Ma, *Chem. Eng. J.*, **174** , 489 (2011).
20. Y. F. Xie, D. Y. Qian, D. L. Wu and X. F. Ma, *Chem. Eng. J.*, **168**, 959 (2011).
21. Y. Bulut and H. Aydin, *Desalination*, **194**, 259 (2006).
22. J. M. Wang, C. Li, H. Zhuang and J. H. Zhang, *Food Control*, **34**, 372 (2013).